2013

AMO-Forced Regional Processes Affecting Summertime Precipitation Variations in the Central United States

Michael C. Veres
University of Nebraska-Lincoln, michael.veres@yahoo.com

Qi Hu
University of Nebraska-Lincoln, qhu2@unl.edu

AMO-Forced Regional Processes Affecting Summertime Precipitation Variations in the Central United States

MICHAEL C. VERES

Department of Earth and Atmospheric Sciences, University of Nebraska at Lincoln, Lincoln, Nebraska

QI HU

Department of Earth and Atmospheric Sciences, and School of Natural Resources, University of Nebraska at Lincoln, Lincoln, Nebraska

(Manuscript received 16 November 2011, in final form 30 May 2012)

ABSTRACT

Numerous previous studies have provided insight into the influence of the Atlantic multidecadal oscillation (AMO) on North American precipitation. However, these studies focused on large-scale processes, and additional studies are needed to gain understanding of local and regional processes that develop in different phases of the AMO and substantiate its influences on precipitation. In this study, the Weather Research and Forecasting (WRF) regional model is used to examine AMO-forced local and regional processes and how they have affected summertime precipitation variation in the central United States.

While moisture transport and convergence by the Great Plains low-level jet have been recognized as necessary conditions for summer precipitation, model simulations show similar low-level moisture flux convergence in the central United States between the cold and warm phases of the AMO. However, there was a strong moistening in the lower troposphere during the AMO cold phase, making the atmosphere more unstable for convection and precipitation. The source of the moisture was found to be a strong positive surface evaporation–precipitation feedback initiated and sustained by increased relative vorticity along a frontal zone. Along the frontal zone, isentropic stretching of the upper-level atmosphere and cyclonic circulation anomalies increased the relative vorticity during the AMO cold phase, providing the dynamic support needed to release the low-level moist instability and produce the increased precipitation. These results indicate that the dynamics of the circulation in the AMO cold phase played key roles to organize regional vorticity processes that further sustained a coupling of precipitation and the surface evaporation and perpetuated the precipitation.

1. Introduction

In the central United States, summer precipitation anomalies strongly affect agricultural production, the environment, and society by damaging floods or straining water supplies and enhancing the risk of wildfires during drought. It would be possible to mitigate some of the consequences of the precipitation anomalies if they can be better understood and predicted accurately. To do this would require a more extensive understanding of the physical processes causing the precipitation anomalies. To gain such an understanding, regional-scale circulations must be examined in addition to the continental-scale circulations, such as those described by general circulation models (GCMs). It is these regional processes that influence regional weather and climate.

Several regional processes have been recognized as contributing to precipitation anomalies in the central United States. The low-level southerly moist flow from the Gulf of Mexico is a major one (e.g., Rasmusson 1967; Arritt et al. 1997; Mo et al. 1997, 2009). As the southerly moist flow is concentrated in a channel from the Gulf of Mexico, it is frequently referred to as the Great Plains low-level jet (LLJ; e.g., Bonner 1968). It has been shown that variations of the geographical location and intensity of the LLJ are directly related to the variations in spring and summer precipitation in the central United States (e.g., Bell and Janowiak 1995; Arritt et al. 1997; Higgins et al. 1997). Tuttle and Davis (2006) further showed that

Corresponding author address: Dr. Qi Hu, 707 Hardin Hall, University of Nebraska at Lincoln, Lincoln, NE 68583-0987.
E-mail: qhu2@unl.edu

DOI: 10.1175/JCLI-D-11-00670.1

the exit region of the LLJ is a favorable area for summertime convective precipitation development.

Regional processes associated with changes in the intensity and position of the upper-level westerly jet and related relative vorticity are other major processes. For example, during the 1993 floods in the central United States and the Midwest, the jet stream was found to be stronger than average and shifted southward from its climatological position, and there was strong regional advection of positive relative vorticity from the northwestern to the central United States (Bell and Janowiak 1995; Trenberth and Guillemot 1996; Mo et al. 1997). The southward shift of the stronger jet displaced the seasonal storm track to the south, making it easier for storms along the storm track to access the low-level moisture in the southerly flow from the Gulf of Mexico. With the vorticity anomalies enhanced regional storms contributed to increasing summertime precipitation in the central United States. Trenberth and Guillemot (1996) also identified an inverse process during the severe drought of 1988.

While revealing the contributing factors influencing precipitation anomalies and extreme precipitation events in the central and the U.S. Midwest and their interrelationship with anomalies in other regions, these studies emphasized that local and regional processes are essential for us to gain detailed understanding of regional precipitation variations. These processes constitute the large-scale circulation anomalies driven by internal and external forcings. Understanding these processes and their relationship with the forcings can therefore improve our ability to describe these processes and to predict regional precipitation and extreme events.

Some of the forcings of the central U.S. summertime precipitation variations have been attributed to anomalies of the sea surface temperatures (SSTs) of the Pacific and Atlantic Oceans (e.g., Namias 1959; 1965; 1969; Namias et al. 1988; Bjerknes 1964; Frankignoul 1985; Lau and Nath 1994, 1996; Latif and Barnett 1994; Seager et al. 2000; Kushnir et al. 2002; Ting and Wang 1997; Hu and Feng 2001, 2008; Mo et al. 2009; Wang et al. 2008, 2010; Hu et al. 2011; Feng et al. 2011). Hu and Feng (2001) showed that the North Pacific SST anomalies are regulating the impacts of tropical SST variations associated with El Niño–La Niña on summertime precipitation variations in the central United States. McCabe et al. (2004) further suggested that the Pacific decadal oscillation (PDO) accounts for 24% of the drought variance in the continental United States. They also showed that the Atlantic multidecadal oscillation (AMO; Mestas-Nunez and Enfield 1999; Kerr 2000) accounts for 28% of the U.S. drought variance. The AMO is a 60–80-yr variation in the North Atlantic SST (Enfield et al. 2001). Although only about two complete cycles of the AMO have been observed in modern instrumentation data, the SST variations at the multidecadal time scale in the North Atlantic have been simulated in long-term GCM simulations (e.g., Knight et al. 2005) and observed in climate reconstructions using tree-ring data and other proxy records of the past 7000 yr (Gray et al. 2004; Feng et al. 2011).

The impact of North Atlantic SST forcing on North American precipitation has been analyzed by using observed anomalies (e.g., Enfield et al. 2001; Schubert et al. 2004; Hu and Feng 2008; Feng et al. 2011) and GCM simulations using idealized SST anomalies (e.g., Sutton and Hodson 2005, 2007; Hu and Feng 2007; Feng et al. 2008; Hu et al. 2011). The general consensus is that warmer SST in the North Atlantic Ocean during the warm phase of the AMO produces below average summertime precipitation in the central United States. Schubert et al. (2004) attribute the 1930s ''Dust Bowl'' era drought to warmer North Atlantic SST. In general, the warmer SST weakens the North Atlantic subtropical high pressure (NASH) and modifies the LLJ on the western flank of the NASH and circulation over North America (Dong et al. 2006; Hu et al. 2011). During the cold phase of the AMO, summer precipitation in the central United States is generally found to be above average (Sutton and Hodson 2005; Hu and Feng 2008).

Interactions of the AMO with other SST forcings, such as El Niño and La Niña, and their effects on North American precipitation also have been examined recently (Schubert et al. 2009; Mo et al. 2009; Hu and Feng 2012). All these studies show very dry conditions in the central and south-central United States in La Niña during the warm phase of the AMO, a result consistent with previous studies showing enhanced droughts in those regions during La Niña (Hoerling and Kumar 2003) or in the warm phases of the AMO (Hu and Feng 2008). There are differences, however, for precipitation anomalies in the other joint phases of the AMO and ENSO. For example, the results in Mo et al. (2009) suggest that above-average precipitation in North America develops in El Niño years in the cold phase of the AMO, while the results in Hu and Feng (2012) show a near-average summertime precipitation in North America in such a situation. As suggested in Hu and Feng (2012), these differences could have resulted from the differences in analyses (e.g., effects on summertime precipitation versus annual precipitation) between those studies. Those differences point to needs for further investigations to clarify them and

for better understanding of the effects of ENSO and the AMO.

While these studies are advancing our knowledge of individual and collective effects of the AMO and ENSO on atmospheric circulation and precipitation, they have brought us only the large-scale effects of those forcings. The local and regional processes that develop within the large-scale circulation environment driven by those forcings are essential for causing the observed precipitation anomalies and need to be understood for improving predictions of regional precipitation and extreme events. This current research is focusing on the regional processes in North America driven by the AMO and intends to provide in-depth understanding of the AMO forcing on the summertime precipitation variations in the central United States. The method used in this study is a regional model, which allows us to simulate regional and mesoscale processes that are too small in scale to be sufficiently resolved and described in coarser-resolution GCMs. It is potentially through these regional and mesoscale processes that the large-scale forcings, such as the AMO, are capitalized in regions to produce the observed precipitation anomalies and extremes.

The regional model and data used in this study are described in detail in the next section (section 2). In section 3, results from testing and validation of the model are presented and discussed. These results provide support for applying this model to study the regional effects of the AMO. After the validation, model experiments and results are described and evaluated in section 4 and, based on these results, a mechanism is proposed to explain development of the major regional processes by which the AMO influences central U.S. summertime precipitation. Major conclusions are contained in section 5.

2. Data and methods

a. Data

The observed monthly precipitation data developed at the Global Precipitation Climatology Centre (GPCC; Beck et al. 2005; Rudolf and Schneider 2005; Rudolf et al. 2003, 2005) were used in this study. The GPCC data are a globally gridded dataset at 0.5° × 0.5° latitude and longitude resolution and span from 1951 to 2004. Also, monthly and 6-hourly atmospheric data from the National Centers for Environmental Prediction–National Center for Atmospheric Research (NCEP–NCAR) reanalysis (Kistler et al. 2001; Kalnay et al. 1996) were used. The NCEP–NCAR reanalysis data are from 1948 to the present. The data are globally gridded with resolutions of 2.5° × 2.5° in latitude and longitude and contain 17 pressure levels in the vertical direction. Even though the NCEP–NCAR reanalysis data are not observations per se, they are derived from and are tightly constrained by observations. For this study, the mean monthly winds and geopotential heights from these data will be analyzed at three pressure levels: 850, 500, and 300 hPa.

Another dataset used in this research is from the outputs of the NCAR Community Atmosphere Model, version 3.1 (CAM3.1) experiments performed by Hu et al. (2011). In their experiments, the CAM3.1 was run with constrained global SST for warm and cold phases of the AMO. The results presented in Hu et al. (2011) were based on the first 20 yr of model integrations for each phase of the AMO, but these model runs were extended to 50 yr in length. It is this extended dataset that was used in part for our study. The resolution of the data produced by Hu et al. (2011) is T42, equivalent to 2.8° × 2.8° in latitude and longitude resolution, and data are available at 6-hourly intervals. Unlike the NCEP–NCAR reanalysis, which incorporates all the forcings that occur in the real atmosphere, the AMO-only-forced GCM data provide a comprehensive dataset of atmospheric variables that vary only by processes driven by the North Atlantic SST anomalies related to the AMO.

b. Methods: The regional model

To identify the AMO-forced regional and mesoscale processes and mechanisms over the central United States that produce the observed and modeled boreal summer [June–August (JJA)] precipitation anomalies we used the regional model, the Advanced Research Weather Research and Forecasting model (ARW-WRF), version 3.1 (Skamarock et al. 2007).

Two nested domains were used in the model setting, an outer domain and an inner domain (Fig. 1). The feedback option between the inner and outer domains was not used. In the early stages of this study, the feedback option was used, and the result showed precipitation of magnitudes much weaker than the observed. After further evaluations of the feedback process, it was deemed incapable to describe the interactions of the domains and therefore was removed.

The outer domain of the model has a resolution of 48 km × 48 km and contains nearly all of North America, from southern Mexico (around 15°–20°N) to northern Alaska and the Queen Elizabeth Islands (around 65°–75°N). The western and eastern boundaries of the outer domain vary widely as the native map projection for the domain is Lambert conformal. In general, the western and eastern boundaries lay approximately 20° of longitude off the coasts of the continental United States. The

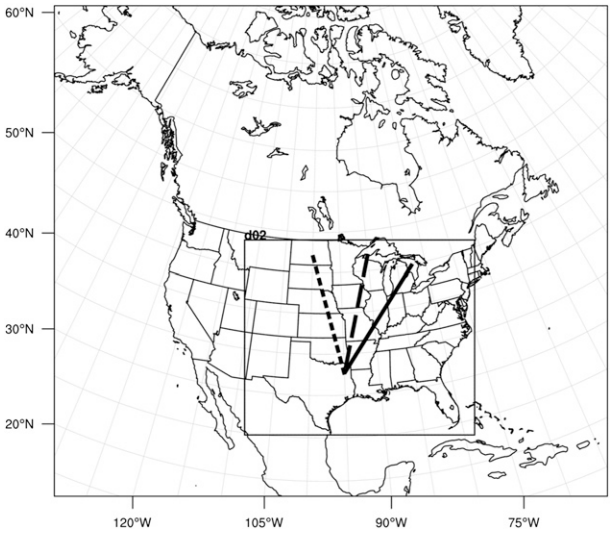

FIG. 1. The two domains used in this study. The outer domain includes the entire image and the inner domain (d02) is bounded by the heavy black box. The three lines inside the inner domain are the three cross sections discussed in section 4.

primary purpose for using an outer domain much larger than the inner domain (Fig. 1) is to provide adequate distance between the boundaries of the two domains so to prevent, as much as possible, the boundary forcing on the outer domain from having large and somewhat direct effect on the boundaries of the inner domain. By limiting this boundary effect, the model will have a greater freedom in developing the internal physical processes in response to the AMO forcing.

The inner domain has a finer resolution of 12 km × 12 km, which allows for development of small-scale surface and atmospheric processes within the domain. The inner domain encompasses nearly all of the continental United States east of the Rocky Mountains, with only the omission of part of eastern New England. The southern boundary starts near 25°N and includes the northern half of the Gulf of Mexico. The northern boundary is approximately parallel to the U.S.–Canadian border in the western half of the domain and includes the far southern reaches of the Ontario and Quebec provinces of Canada in the eastern half of the domain. The western and eastern boundaries of the inner domain are approximately at 110°W in the west and along the Atlantic coast of the continental United States in the east (70°–78°W). Expanding the boundaries of the inner domain beyond these limits was not feasible, as the boundaries were near the limits of the available computation capabilities.

All WRF runs performed in this study used identical domains and model parameters. The model was run using the Noah land surface model and Monin–Obukhov surface physics options and the Kain–Fritsch (KF) parameterization scheme for atmospheric convection. Model output is at 3-h intervals.

3. Model validation

Before using WRF to examine the AMO-forced regional processes and precipitation, we need to verify that the model is capable of producing realistic atmospheric circulations and precipitation in the study region during the AMO.

The NCEP–NCAR reanalysis data were used to force the regional model for five specified summers from each phase of the current AMO cycle, for a total of 10 summer seasons. According to Hu and Feng (2008) (see their Fig. 6), the cold phase of the AMO was from 1961 to 1990 and the warm phase was from 1991 to 2009. In selecting the 10 yr for the validation, we used the results of Hu and Feng (2008), which showed that the central United States (Kansas, Nebraska, Iowa, and Missouri) experiences increased (decreased) precipitation during the cold (warm) phase of the AMO. However, as Ruiz-Barradas and Nigam (2005) showed the correlation between the observed and the NCEP–NCAR reanalysis precipitation is weak in the Great Plains and, when compared to the observations, the NCEP–NCAR reanalysis data show a bias toward increased summer precipitation during the previous 30 yr. Recognizing this bias, we focused on years when both the observations and the NCEP–NCAR reanalysis were indicating increased (decreased) precipitation during the cold (warm) phase of the AMO. Of these years, the ones with the greatest precipitation anomalies were selected. The low correlation between the observations and the NCEP–NCAR reanalysis also required that the presence of El Niño or La Niña not be a deciding factor. The years selected through this process for the model validation were 1965, 1966, 1979, 1981, and 1986 for the AMO cold phase and 1999–2003 for the AMO warm phase.

For each selected year, WRF was run from 16 May to 1 September in each simulation. The first 2 weeks of each model run was discarded as model spinup. These results were then compared to observations to evaluate the effectiveness of the model at simulating the observed conditions.

We note that because five years in the warm phase and five years in the cold phase of the current AMO cycle were used in the validation simulations, there was no ''control run.'' As such, the anomalies were calculated by removing the average of all 10 simulations from each simulated year. The equal number of years from the cold and warm phases resulted in mirror images for anomalies for the cold and warm phases of the AMO.

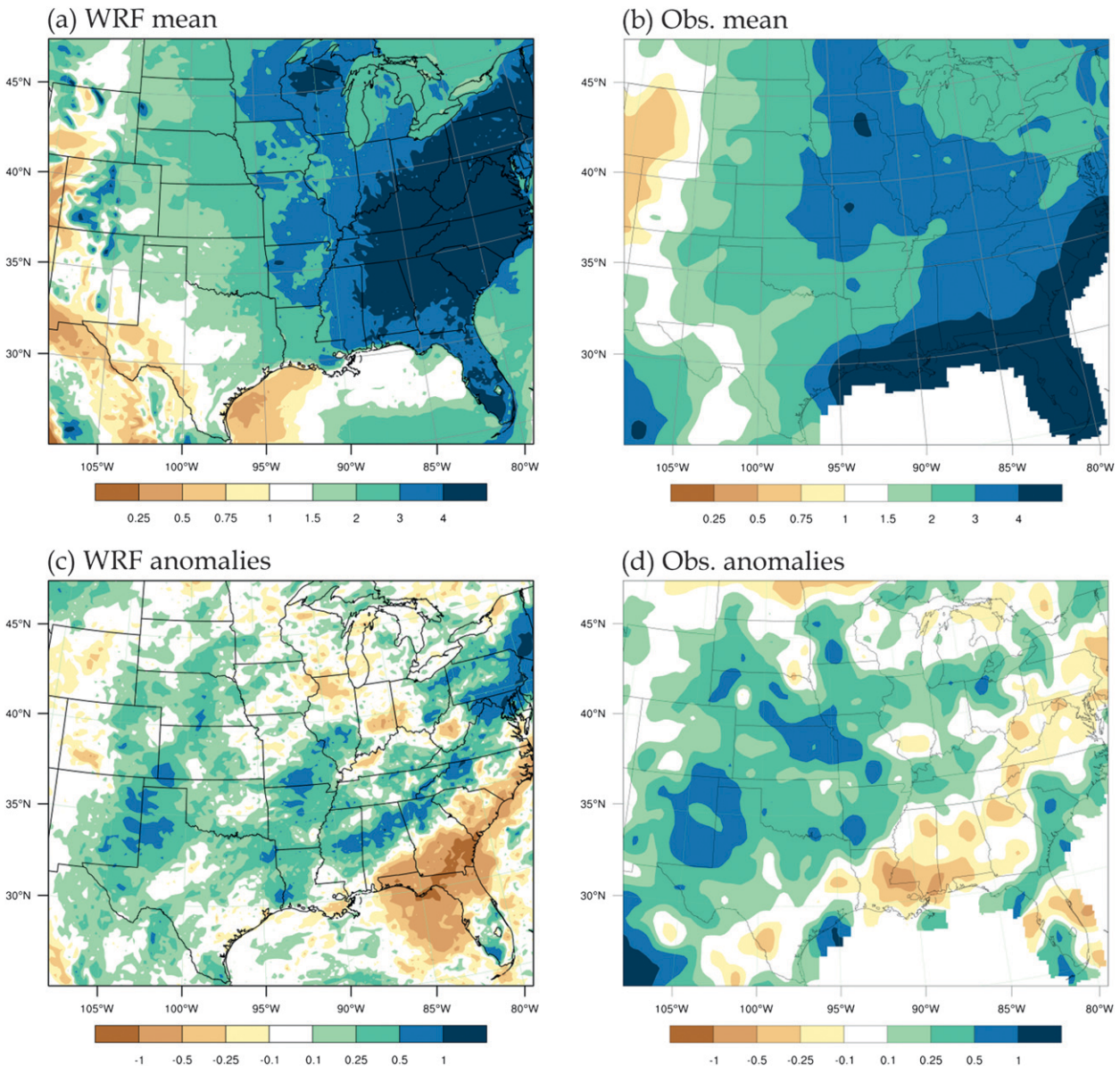

FIG. 2. Mean (10 yr) JJA precipitation for (a) NCEP–NCAR reanalysis–forced WRF simulation and (b) observations. (c) Simulated and (d) observed precipitation anomalies in the cold phase of the AMO. Units are in millimeters per day.

The following discussions primarily focus on the anomalies in the cold phase of the AMO.

Also in the following discussions, we use ''central United States'' for the region encompassing Kansas, Nebraska, Missouri, and Iowa; ''south-central United States'' for Texas, Oklahoma, western Louisiana, and Arkansas; ''north-central United States'' for North and South Dakota and Minnesota; and ''the Midwest'' for Wisconsin, Illinois, Indiana, Michigan, and Ohio. In addition, specific states will be mentioned when needed for clarity.

The model-simulated and observed precipitations are shown in Fig. 2. Comparisons of these results show simulated precipitation consistent with observations in most of the study region in both the 10-yr means (Figs. 2a versus Fig. 2b) and cold phase of the AMO (Fig. 2c versus Fig. 2d). The precipitation magnitudes are also consistent throughout much of the model domain (Fig. 2a versus Fig. 2b). During the AMO cold phase, however, there is a disagreement in precipitation anomalies in the east and southeast United States (Fig. 2c versus Fig. 2d). While the observations show a band of negative

anomalies of precipitation from east of Pennsylvania down to Louisiana, the simulations show positive anomalies across that region. In the simulation result, a band of negative precipitation anomalies is found along the southeast coasts of the United States and across Florida. This misplaced dry band also causes discrepancy with the observed narrow band of positive precipitation anomalies along the coastal areas and northern Florida. The displacement of the simulated anomalies toward the coastal area is likely the result of the model producing more zonal flow in the southern United States. This zonal flow traps more moisture from the Gulf of Mexico in the southern United States, likely increasing the precipitation and producing the simulated positive anomalies in Mississippi, Louisiana, and Georgia during the cold phase of the AMO. While the displaced anomalies indicate model limitations in simulating precipitation in the east coastal regions, the model appears to be reasonably consistent in simulating precipitation in the central, north and northeastern United States, as the simulated anomalies in those regions are consistent with the observations.

It should also be noted that the model does not capture the observed nocturnal peak in diurnal precipitation in the Great Plains (Wallace 1975). This is likely due to the poor representation of the diurnal cycle by the Kain–Fritsch cumulus parameterization scheme used in the WRF model (Liang et al. 2004). However, our analysis of the diurnal cycle of the model-simulated precipitation indicates approximately an equal amount of precipitation between local daytime (1200–0000 UTC) and nighttime (0000–1200 UTC) contributing to the daily precipitation. The same result appeared in both the years selected for the AMO warm and cold phases. These results suggest that the simulated daytime and nocturnal response to the AMO forcing is similar and that a shift toward more nocturnal precipitation would not alter the simulated daily to seasonal precipitation shown in Fig. 2c. In other words, the inaccuracy in describing the diurnal cycle of precipitation caused by the KF scheme is not important in this study.

To evaluate the model simulation of the atmospheric circulations, we compared the simulated and observed winds and geopotential heights at 850, 500, and 300 hPa (Fig. 3). Overall, the model is able to reasonably reproduce the observations. During the AMO cold phase, the primary feature at 850 hPa in the observations and simulations is an anomalous wave pattern in the geopotential heights (Figs. 3a,d) with the least negative (more negative) anomalies in the southeastern (north central) United States, although the wave is more meridional in the simulations, producing wind anomalies that are more zonal in the south-central United States. Besides this minor difference, the model simulation is consistent with the observation in the lower troposphere.

At 500 and 300 hPa, the cold phase geopotential height anomalies display an anomalous wave pattern in both the observations (Figs. 3b,c) and simulations (Figs. 3e,f). This pattern is similar to the one at 850 hPa, with the most positive (negative) anomalies occurring in the southeast (north central) United States.

To summarize, the regional model simulations generally produced similar results in both magnitude and distribution to observations. The model simulated the mid- and upper-level anomalous circulations reasonably well in the study domain. At the low level, the accuracy was weaker. However, the overall pattern of an anomalous high pressure in the southeastern United States and low pressure over the central United States during the cold phase of the AMO was reproduced. The model also simulated the observed increase in precipitation in the central United States during the cold phase of the AMO, albeit the agreement between the simulations and the observations was weaker in the Midwest. These overall performances of the model show that it was able to describe major physical processes that produced the study phenomena. Additional details of the differences between the observation and model simulations and more discussions of model ability in describing the phenomena of interest to this study were documented in Veres (2011).

4. Model experiments and results

We next used the model in a series of experimental simulations. These simulations were forced by GCM outputs with specified (constant) SST anomalies describing the AMO in the North Atlantic Ocean and climatological SST elsewhere (Hu et al. 2011). The details on the SST distributions used to drive the GCM simulations are shown in Fig. 1 of Hu et al. (2011). Outputs of five GCM simulation years for the warm or cold phase of the AMO from Hu et al. (2011) were used to drive the WRF experiments. The five years for the cold (warm) phase of the AMO were selected in a manner consistent with the NCEP–NCAR reanalysis forcing; that is, the five wettest (driest) years in the cold (warm) phase of the AMO were used. Because only AMO-driven large-scale circulations were used to force the regional model, by analyzing the regional model simulations forced in different phases of the AMO we can identify the AMO-driven regional-scale dynamic processes and associated summertime precipitation variations in the central United States.

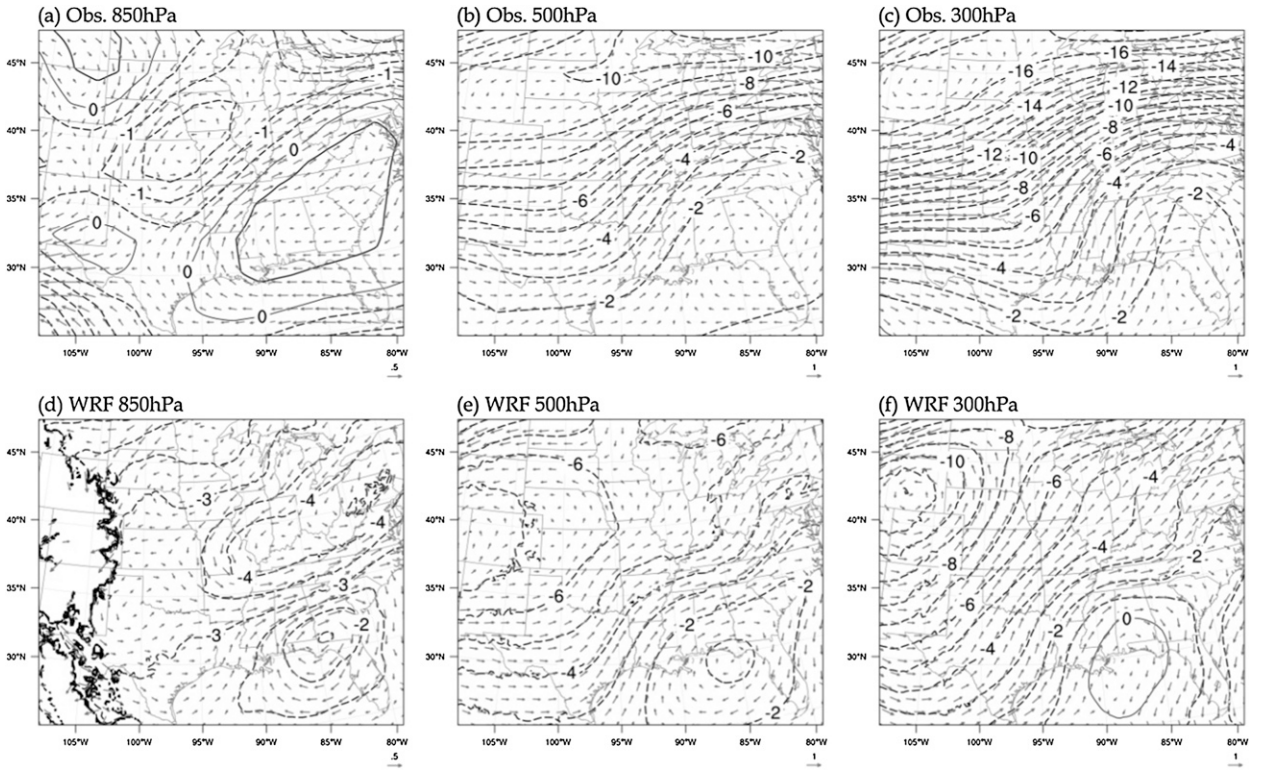

FIG. 3. (a)–(c) Observed and (d)–(f) simulated JJA (a),(d) 850-, (b),(e) 500- and (c),(f) 300-hPa wind and geopotential height anomalies for the cold phase of the AMO using the five selected years for the cold phase (1965, 1966, 1979, 1981, and 1986). Units are in meters per second for winds and meters for geopotential height. Reference vectors are (a),(d) 0.5 and (b),(c),(e),(f) 1 m s^{-1}. Contour intervals are (a),(d) 0.5 and (b),(c),(e),(f) 1 m with labels every other contour. Solid (dashed) lines indicate positive (negative) anomalies.

Figures 4a,b show the model-simulated AMO-forced JJA 10-yr mean and cold phase anomalous precipitation, respectively. Comparisons of Fig. 4a with the NCEP–NCAR reanalysis–forced precipitation in Fig. 2b indicate that the model produced less precipitation in the central United States, the Midwest, and particularly in the south-central United States. Despite the reduced magnitudes, the spatial pattern of the mean precipitation in the study region is similar to the observed 1971–2000 climatology (Fig. 4c), with precipitation generally increasing toward the north and the east. Both the simulations and observations display similar regions of higher precipitation that extend meridionally from Minnesota and Wisconsin to around the Missouri–Arkansas border and taper off toward the west. The westward gradient is stronger in the simulations, but the overall pattern outside the south-central United States is similar. Despite the smaller magnitude in the JJA mean precipitation, the simulated cold phase precipitation anomalies (Fig. 4b) agree fairly well with previously described AMO-forced patterns (e.g., Enfield et al. 2001; Hu et al. 2011). Much of the central and eastern United States experiences above-average precipitation while the southeastern United States (e.g., Florida) has below-average precipitation. Changes in summertime precipitation in these regions between the cold and warm phases of the AMO are statistically significant at the 95% confidence level (shown in the hatched area in Fig. 4b). These anomalies display a strong similarity to the NCEP–NCAR reanalysis–forced model simulations (Fig. 2c), despite the fact that NCEP–NCAR reanalysis–forced simulations have all possible forcings, besides the AMO. This similarity thus suggests that the AMO influence is playing a dominant role in summertime precipitation variations in North America at the multidecadal time scale. The opposite precipitation anomalies were simulated by the model driven by the warm phase AMO forcing.

To examine the regional and local processes that may have contributed to these contrasting precipitation anomalies between the cold and warm phase of the AMO, we start with the analysis of the moisture processes. As shown in many prior studies (e.g., Arritt et al. 1997; Higgins et al. 1997), changes in moisture content

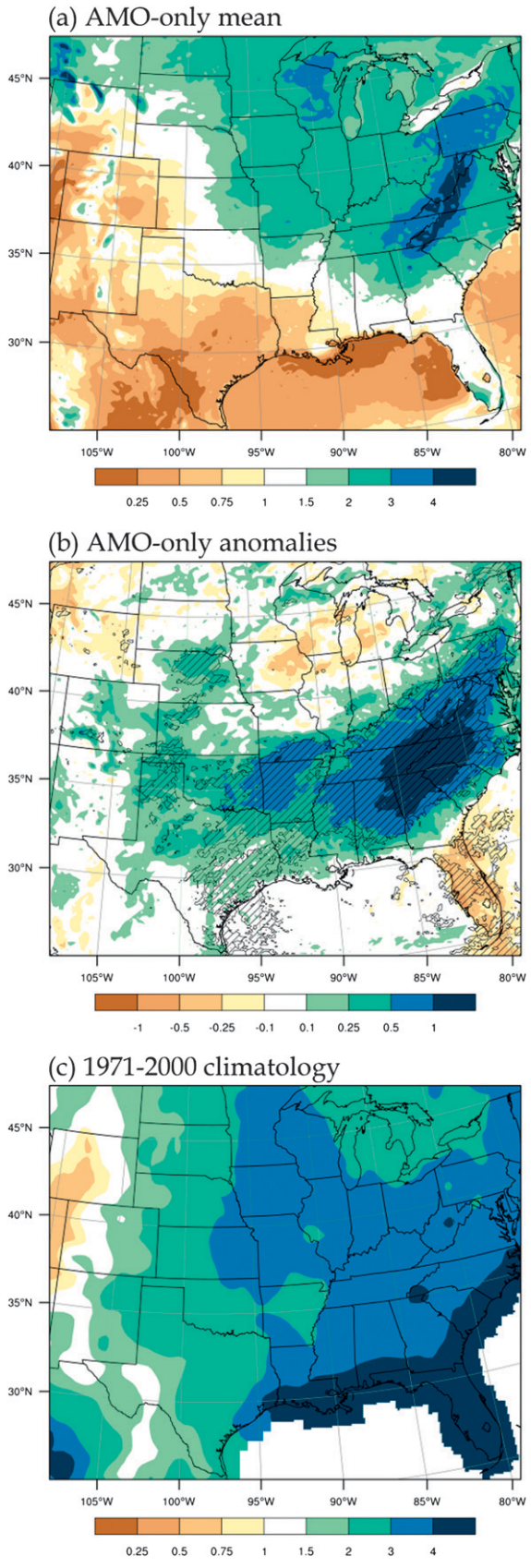

of the lower troposphere can have a strong impact on precipitation. Figure 5 shows the JJA surface–700-hPa integrated moisture flux divergence in the study domain. Interestingly, low-level moisture convergence is shown in the central United States and neighboring areas in the Great Plains during both the cold (Fig. 5a) and warm phase (Fig. 5b) of the AMO. The similar moisture convergence in the central United States in Figs. 5a,b indicates the general availability of moisture in the lower troposphere during JJA in either the cold or the warm phase of the AMO. The similarities in low-level moisture convergence between the cold and warm phases of the AMO indicate that different dynamic process must be active, such that those processes in the cold phase of the AMO would make the atmosphere more efficient in converting moisture into precipitation and sustain the increase in JJA precipitation.

To identify those processes that make the atmosphere more conducive to storm development in JJA, we first examine the thermodynamic profile of the atmosphere in the cold and warm phases of the AMO. An unstable profile is essential for convective storms, which are the primary form of JJA precipitation in the central United States. Figure 6 shows three vertical cross sections of moisture anomalies. All three cross sections share a common southern endpoint in northeast Texas and diverge toward the north, terminating in Michigan, Wisconsin, and North Dakota. They will be referred to as eastern, central, and western cross sections and are identified in Fig. 1 by solid, dashed, and dotted straight lines, respectively. Intriguingly, all three cross sections show moistening in the layers below 700 or 750 hPa and drying aloft during the cold phase of the AMO. A reversed moisture anomaly profile occurs during the warm phase of the AMO. The moistening in the lower troposphere and drying aloft in the cold phase reduce the moist static stability of the atmosphere, making it more convectively unstable and prone to convection and precipitation.

Additional features in spatial variation in the moisture profile of importance to precipitation are evident from comparisons of Figs. 6a–c. In the western cross section (Fig. 6c), the enhanced low-level moisture covers a much greater extent into the higher latitudes than in the eastern cross section (Fig. 6a). Positive

←

FIG. 4. JJA (a) 10-yr mean precipitation and (b) cold phase anomalies for the AMO-forced WRF simulations. (c) The 1971–2000 precipitation climatology. The same scales are used as in Fig. 2. Units are in millimeters per day. For (b), the hatched pattern indicates statistical significance at the 95% confidence level.

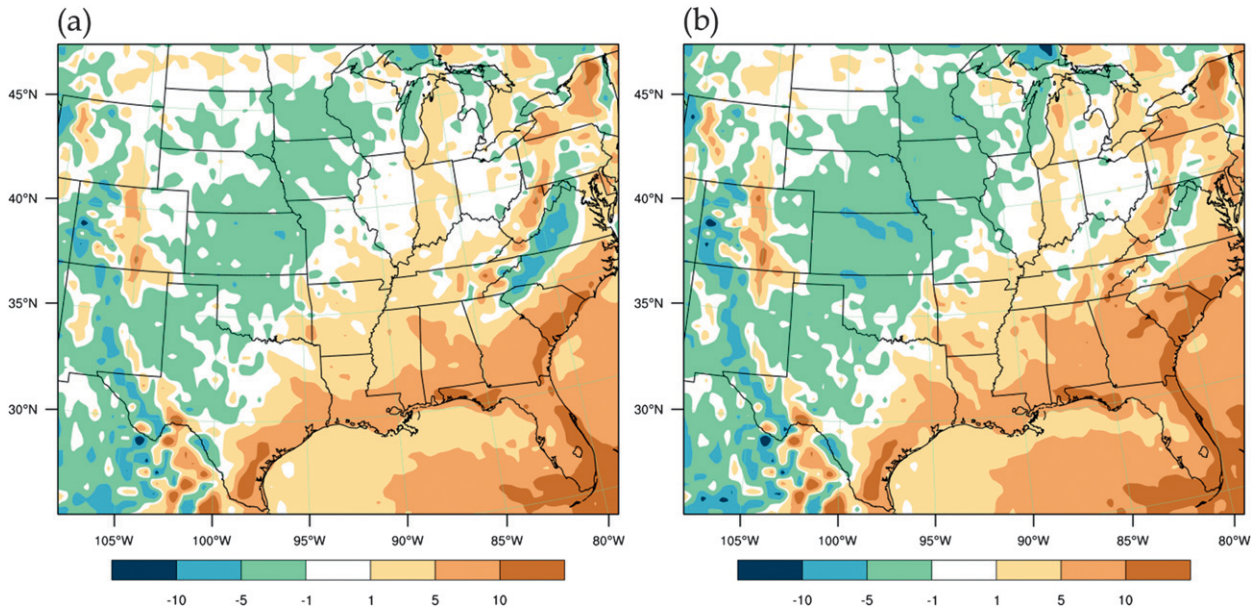

FIG. 5. JJA mean moisture divergence for (a) cold and (b) warm phase of the AMO. Positives are divergence. Units are in 10^{-6} kg s^{-1} m^{-2}.

moisture anomalies also extend farther into the mid-troposphere. These features indicate more moistening in the central Great Plains in the cold phase of the AMO. Comparisons of the three cross sections further reveal that the vertical gradient of moisture is more prevalent in the eastern and western cross sections and less prevalent in the central cross section. In accordance with these moisture anomalies across these regions, strong positive precipitation anomalies were observed in Nebraska as well as in Arkansas (Fig. 4b). The results show good agreement between the decreased moist static stability and increased precipitation during the AMO cold phase and suggest that the AMO-forcing produces an environment that is less stable for convection and more efficient in converting the moisture into precipitation.

The source of the drier air aloft in the cross sections in Fig. 6 is most likely the process presented in Hu et al. (2011). They suggest that during the AMO cold phase the maritime air mass from the Gulf of Mexico intrudes northward and produces a frontal zone with the pre-existing continental air mass to the north. While this may reasonably explain the drier mid- and upper-level air, what may be causing the moistening in the lower troposphere? According to Fig. 5, the low-level moisture flux convergence from the southerly flow is similar between the cold and warm phase of the AMO. This similarity suggests some additional moistening process initiated/sustained by the frontal process during the cold phase of the AMO.

Such process may be identified by examining the atmospheric water budget given as $d(\rho q)/dt = E - P - \mathbf{V} \cdot (\rho q \mathbf{V})$. In this budget, E is the surface evaporation, P is the precipitation, $\mathbf{V} \cdot (\rho q \mathbf{V})$ is the horizontal moisture divergence, ρ is air density, q is the vapor mixing ratio, and $\mathbf{V}$ is horizontal velocity. According to the atmospheric water budget, when there is little variation in moisture flux convergence between two environments, the surface evaporation E can make the difference for changes in atmospheric moisture content $d(\rho q)/dt$ and precipitation between the two environments. Figure 7a shows the JJA anomalies of surface evaporation in the cold phase of the AMO. Indeed, positive anomalies are shown across the central United States where an increase in lower troposphere moisture was shown in Fig. 5. Particularly, the strongest positive E anomaly in the central United States is near Arkansas with a secondary maximum in Nebraska. The consistent increase in surface evaporation and moistening in low-level atmosphere in the cold phase of the AMO in the absence of a strong difference in low-level moisture flux convergence between the cold and warm phase of the AMO (Fig. 5) suggests a strong positive feedback of surface evaporation and precipitation in the cold phase of the AMO. In this feedback, the moistening in the lower troposphere and drying aloft and their induced weakening in static stability of the atmosphere contribute to convection and precipitation development, which in turn maintains the soil moisture and surface evaporation. The coupling of the surface evaporation and

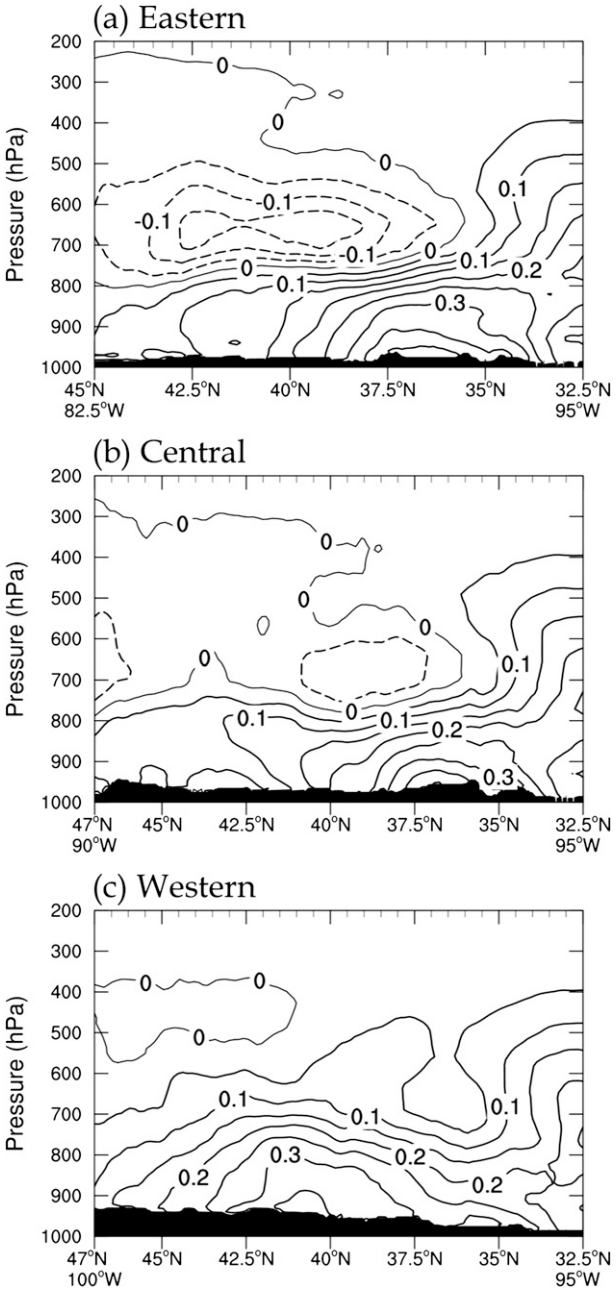

FIG. 6. JJA cold phase moisture anomalies for (a) eastern, (b) central, and (c) western cross sections. Units are in grams per kilogram. Contour interval is 0.05 g kg^{-1} with labels every 0.1 g kg^{-1}. Solid (dashed) lines indicate positive (negative) anomalies.

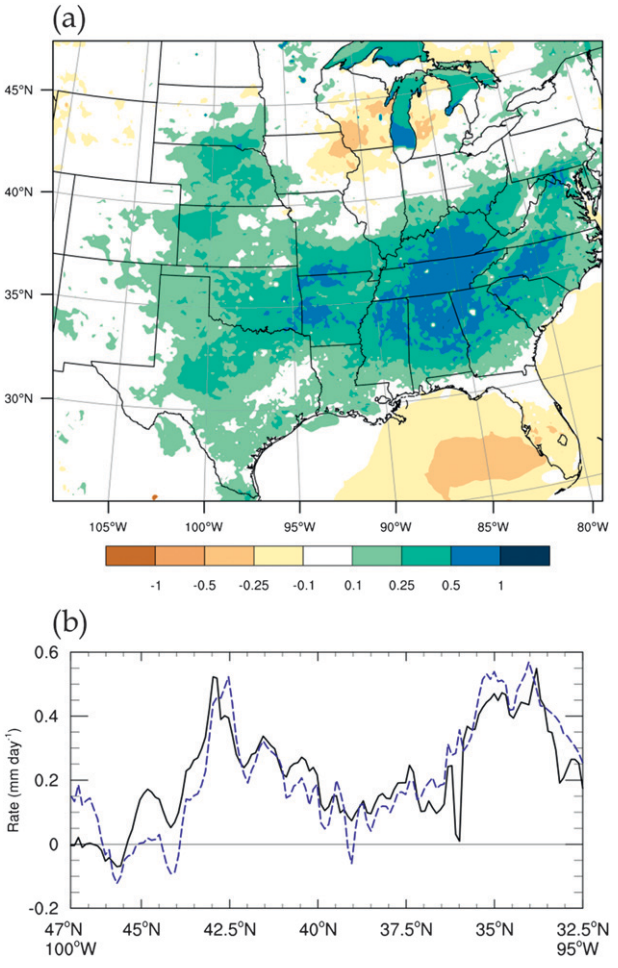

FIG. 7. (a) JJA cold phase anomalies of surface evaporation. (b) Cross section of JJA cold phase anomalies of evaporation (solid line) and precipitation (dashed line). The cross section uses the same endpoints as in Fig. 6c. Units for (a),(b) are millimeters per day.

precipitation, as a result of this feedback and shown clearly in Fig. 7b, sustains the low-level moistening shown in Fig. 6.

While this feedback in the cold phase of the AMO creates a thermodynamic environment favorable for precipitation, it must be organized and sustained by dynamic processes at the regional and larger scales. Such dynamic processes would effectively enhance the instability of the moist atmosphere so that precipitation occurs with the release of the instability. The initial increase in precipitation would start the positive feedback of surface evaporation to the precipitation, and continuing interactions of precipitation and the surface processes would sustain this feedback and precipitation in the cold phase of the AMO. These dynamic processes would have to originate from those that cause the vorticity disturbances in the region. In the following, we will examine these disturbances and their roles in increasing precipitation in the cold phase of the AMO.

One possible cause for increase in the midtroposphere vorticity would be the advection of relative vorticity in the large-scale circulation in North America driven by

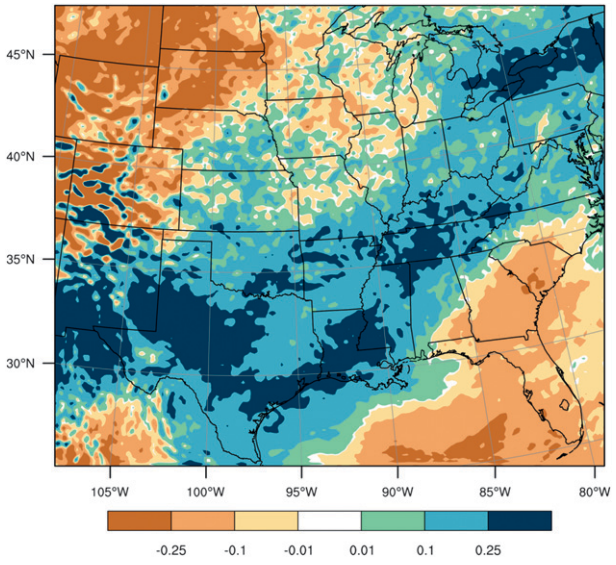

FIG. 8. JJA 500-hPa relative vorticity anomalies in AMO cold phase. Units are 10^{-5} s^{-1}.

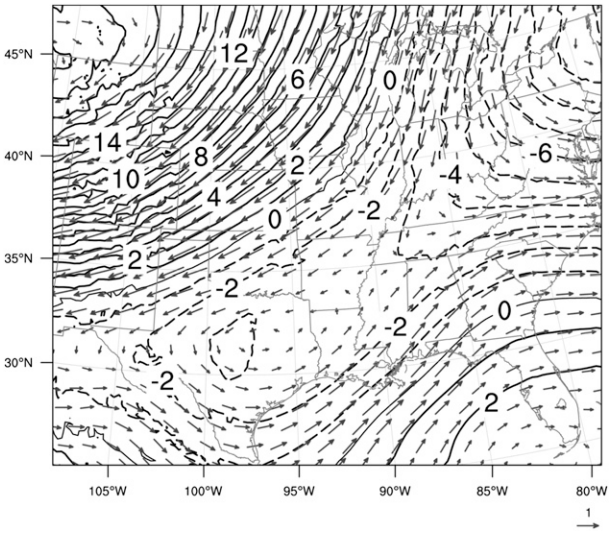

FIG. 9. JJA cold phase 500-hPa geopotential height and wind anomalies. Units are in meters per second for winds and meters for geopotential height. The reference vector is 1 m s^{-1}, and the contour interval is 1 m with labels every 2 m. Solid (dashed) lines indicate positive (negative) anomalies.

the AMO. Figure 8 shows the cold phase JJA 500-hPa relative vorticity anomalies, which show positive anomalies in the central and south-central United States. The positive anomalies agree remarkably well with the precipitation anomalies, especially in the area of Kansas and Nebraska. This agreement indicates the vorticity is a key source for sustaining the feedback process and increase in precipitation during the cold phase of the AMO. According to the vorticity equation, major processes contributing to the increase in relative vorticity would include vorticity advection, divergence, and vorticity generation by vortex stretching. Examining these individual processes in the study region, we found weak cyclonic circulation anomalies over the south-central United States (Fig. 9), where strong vertical motion and precipitation concurred. Farther to the north, however, the curvature of the flow in Fig. 9 indicates neutral or weak negative relative vorticity in the central United States. Our examinations of the vorticity terms indicated that advection of relative vorticity may have played a minor role (cf. the results in Figs. 8, 9) and instead the stretching of the atmospheric vortex may have played an important role to increase the relative vorticity in that region.

By the conservation of potential vorticity, the vertical contraction (stretching) of an atmospheric column–vortex bound vertically by two potential temperature surfaces decreases (increases) the absolute vorticity of the atmospheric column (Holton 2004). This can be seen by analyzing the equation for conservation of potential vorticity in isentropic coordinates,

$$(\zeta_\theta + f)\left(-g\frac{\partial\theta}{\partial p}\right) = \text{const}. \qquad (1)$$

In (1), ζ_θ and f are the relative and planetary vorticity in isentropic coordinates, respectively; g is the gravitational constant; and $-\partial\theta/\partial p$ is the effective depth of the vortex (θ is potential temperature and p is pressure). As g is a constant, (1) dictates that an increase (decrease) in the effective depth must have an equal decrease (increase) in the absolute vorticity, or relative vorticity if we constrain ourselves to zonal flow, for demonstration purposes. It is important to note that effective depth $-\partial\theta/\partial p$ decreases when the vertical atmospheric column Δp stretches.

To show the vorticity generation by this process in the central United States during the cold phase of the AMO, in Fig. 10a we plot the cold phase potential temperature and in Fig. 10b we plot the effective depth anomalies for two different atmospheric columns (one from 600 to 400 hPa and the other from 700 to 400 hPa). In Fig. 10a, in the layer below 700 hPa, negative anomalies of potential temperature increase rapidly toward the east. Between 700 and 500 hPa, the horizontal gradient of the potential temperature anomalies is minimal. Between 500 and 400 hPa, the horizontal gradient once again becomes more noticeable. This profile results in a decrease in $-\partial\theta/\partial p$ in the AMO cold phase, which is shown in Fig. 10b as the air column moves from the west into the central United States. From (1), this change in

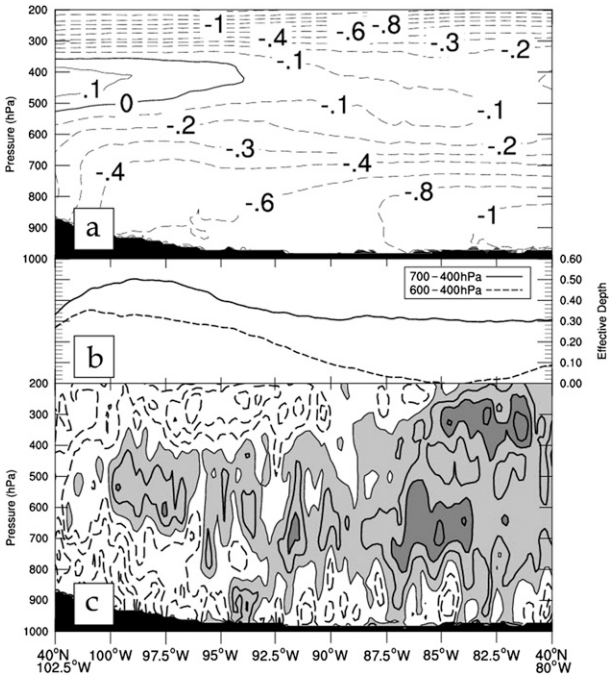

FIG. 10. (a) JJA cold phase potential temperature anomaly cross section at 40°N between 102.5° and 80°W, (b) $-\partial\theta/\partial p$ (effective depth) anomalies between 700 and 400 hPa (solid) and 600 and 400 hPa (dashed), and (c) relative vorticity anomalies along the same cross section. Units are °C in (a), °C Pa^{-1} in (b), and s^{-1} in (c). Contour intervals are 0.2 K (0.1- and 0.3-K contours also included) in (a) and 2×10^{-6} s^{-1} in (c). Solid (dashed) lines indicate positive (negative) contours. In (c), light shading indicates positive values with dark shading indicating values $>2 \times 10^{-6}$ s^{-1}.

$-\partial\theta/\partial p$ would cause an increase in relative vorticity and spinup of the air column.

The positive anomalies in relative vorticity produced by this process are shown in Fig. 10c. While Fig. 10c shows a cross section from 102.5° to 80°W along 40°N, it would also describe vorticity change of a vortex when it travels from the west to the east in the westerlies. In the central United States (95°–102.5°W), the positive anomalies of relative vorticity first develop between 600 and 400 hPa, consistent with the effective depth anomalies between those levels (Fig. 10b). Farther toward the east, the positive relative vorticity anomalies descend to 700 hPa, again consistent with changes in the 700–400-hPa effective depth. Thus, the atmospheric vortex gained more positive relative vorticity while traveling to the east. The stronger positive vorticity in the moistening and unstable environment may have caused increase in convective precipitation and sustained the positive precipitation–evaporation feedback and the positive precipitation anomalies during the cold phase of the AMO. During the warm phase of the AMO, the vortex shrank causing increase in negative vorticity and acted to inhibit precipitation development.

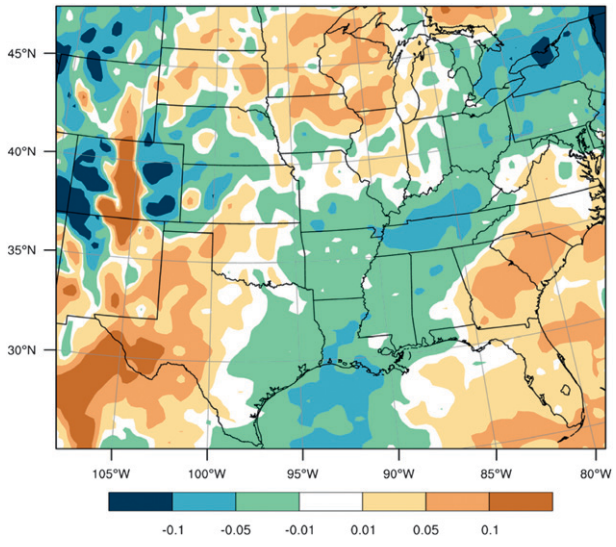

FIG. 11. JJA 400-hPa divergence anomalies for the cold phase AMO-forced WRF simulations. Positive values indicate divergence. Units are 10^{-5} s^{-1}.

The previous discussion of the atmospheric vortex stretching and resulting changes in relative vorticity can also be framed from a perspective of the mid- to upper-level divergence. As shown in Fig. 11, there was a mass convergence anomaly at 400 hPa during the AMO cold phase over most of the central United States, particularly over Kansas, Nebraska, and Missouri. This convergence would lead to a vertical stretching of the atmospheric vortex and generation of the positive relative vorticity shown in Fig. 10c. As the vortex stretches, the increasing positive relative vorticity in the midtroposphere would extend downward and break through the boundary between the moistened low-level air and the overlying drier air, releasing the potential moist instability. These processes are shown in Figs. 10b,c, where the gradual descent of the lower boundary of the vortex occurred following the vortex stretching (Fig. 10b) and the resulting increase in relative vorticity (Fig. 10c) first appeared between 600 and 400 hPa and then extended down to 700 hPa farther to the east. These processes helped promote development of convection and increase in precipitation during the cold phase of the AMO.

The stretching of the midtropospheric vortex is also related to the air temperature anomalies induced by the SST forcing during the cold phase of the AMO. As shown in Fig. 12a, the lower troposphere (850 hPa) has cooler temperatures in much of the central and eastern United States during the cold phase of the AMO. These anomalies in temperature are likely attributable to the intrusion of the maritime air mass from the Gulf of

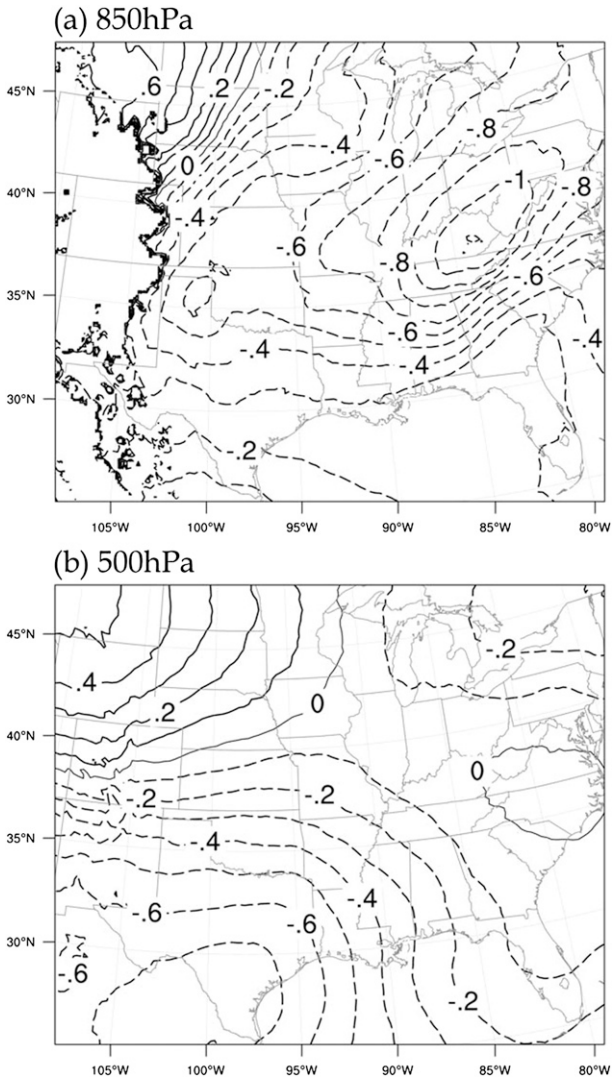

FIG. 12. JJA (a) 850- and (b) 500-hPa temperature anomalies for the cold phase AMO-forced WRF simulations. Units are °C. The contour interval is 0.1 with labels every 0.2. Solid (dashed) lines indicate positive (negative) anomalies.

Mexico into the continental United States. This intrusion created a frontal zone from the west to the east across the central United States, with colder air in the south and warmer air in the north (Fig. 12b). This frontal zone is similar to that found in Hu et al. (2011) in their GCM simulation results and also in the vertical moisture profiles discussed earlier in this study (Fig. 6). The strong baroclinic environment along the frontal zone in the central United States would favor the dynamic processes resulting in stretching of vortices, development of disturbances into severe convection and precipitation, and sustaining the precipitation–evaporation feedback to perpetuate wet summers during the cold phase of the AMO. An absence of such a frontal zone and the associated processes during the AMO warm phase discourages precipitation.

5. Concluding remarks

In this study, we examined the regional mechanisms behind the observed (e.g., Enfield et al. 2001) increases in central U.S. precipitation during the cold phase of the AMO. To this end, we used the AMO-driven GCM simulations from Hu et al. (2011) to force the WRF high-resolution regional model. The regional model simulations suggest that the positive precipitation anomalies during the AMO cold phase in the central United States are largely attributable to a decrease in the moist static stability and enhanced relative vorticity in a favorable dynamic environment.

It was intriguing when it was found that there was little difference in low-level moisture flux convergence in the central United States between the cold and warm phases of the AMO (Fig. 5) but there was strong moistening in the atmosphere below about 700 hPa (Fig. 6). This situation indicates that the large-scale circulations in the cold or warm phase of the AMO did not strongly alter the moisture availability (by not modifying the moisture flux convergence) but rather initiated another process acting to increase the low-level moisture. The moistening was also restricted to the lower troposphere, with normal to drier air above the moist layer. This vertical moisture gradient provided an environment more conducive for precipitation during the AMO cold phase by reducing the moist static stability of the atmosphere. The vertical moisture gradient is also indicative of a frontal zone between an expanded moist Gulf of Mexico maritime air mass and an overriding drier continental air mass.

An important indication of similar low-level moisture flux convergence in the south-central and central United States between the cold and warm phases of the AMO is that increase in moisture in the lower troposphere in that region occurs regardless in the summer months as a consequence of changes in seasonal circulation of the large-scale environment: for example, the emerging and establishment of the southerly low-level jet. What may differentiate the precipitation anomalies between wet and dry summers are the atmospheric dynamic processes. As we have identified in this study, in the cold phase of the AMO the large-scale circulation driven by the SST anomalies in the AMO organizes active dynamic processes that generate the relative vorticity (Figs. 10, 8), initiate precipitation, and sustain low-level moisture and precipitation by further activating a positive feedback between the precipitation and surface evaporation (Figs. 7, 6).

We found that, in addition to the vorticity advection, variations in the rate of isentropic vortex stretching between the cold and warm phases of the AMO induce positive relative vorticity anomalies during the cold phase and negative anomalies during the warm phase. In the cold phase, the positive relative vorticity anomalies created by vortex stretching played a particularly important role in initiating and maintaining the convective instability and precipitation along the frontal zone in the central United States. There are two major sources for the vertical stretching and vorticity variations: differential air temperature anomalies between the lower and middle troposphere (Fig. 12) along the frontal zone and mid- to upper-level mass convergence (Fig. 11). During the AMO cold phase, the stretching of the atmospheric column increases the vorticity. The lower boundary of the vortex extends to 700 hPa, taking positive relative vorticity anomalies downward. With the intrusion of strong positive vorticity from the overlying layer, the boundary capping moisture in the lower troposphere collapses and convection occurs in the conditionally unstable environment. The strong agreement between the relative vorticity anomalies in the middle troposphere and the precipitation anomalies further suggests that the relative vorticity anomalies generated in these processes, or the dynamic properties of the environment, are a primary determinant of the precipitation anomalies in the central United States. This is particularly true around Kansas and Nebraska, where the generation of positive vorticity anomalies may have helped organize the coupling of the precipitation and surface evaporation and sustain the increase in precipitation in the cold phase of the AMO.

In conclusion, the fine-resolution regional model simulations in this study allow for detailed analysis of the local and regional moisture processes and the varying regional mechanisms for vorticity development and causes of the summertime precipitation variations during the AMO. By revealing these regional processes, this study not only complements the existing studies on the AMO effects on summertime precipitation but also assists our comprehension of how such effects have been achieved. These results will be helpful for improving predictions of summertime precipitation in the central United States.

Acknowledgments. We thank Dr. Robert Oglesby and Dr. Song Feng for their useful suggestions during the modeling phase of this study. We would also like to thank three anonymous reviewers and the editor, Dr. Kerry Cook, whose comments led to the improvement of this manuscript. This research has been supported by NOAA Grant NA09OAR4310188 to the University of Nebraska at Lincoln and by the USDA Cooperative Research Project NEB-38-088.

REFERENCES

Arritt, R. W., T. D. Rink, M. Segal, D. P. Todey, C. A. Clark, M. J. Mitchell, and K. M. Labas, 1997: The Great Plains low-level jet during the warm season of 1993. *Mon. Wea. Rev.,* **125,** 2176–2192.

Beck, C., J. Grieser, and B. Rudolf, 2005: A new monthly precipitation climatology for the global land areas for the period 1951 to 2000. DWD Climate Status Rep., 181–190.

Bell, G. D., and J. E. Janowiak, 1995: Atmospheric circulation associated with the Midwest floods of 1993. *Bull. Amer. Meteor. Soc.,* **76,** 681–695.

Bjerknes, J., 1964: Atlantic air-sea interaction. *Advances in Geophysics,* Vol. 10, Academic Press, 1–82.

Bonner, W., 1968: Climatology of the low level jet. *Mon. Wea. Rev.,* **96,** 833–850.

Dong, B., R. T. Sutton, and A. A. Scaife, 2006: Multidecadal modulation of El Niño–Southern Oscillation (ENSO) variance by Atlantic Ocean sea surface temperatures. *Geophys. Res. Lett.,* **33,** L08705, doi:10.1029/2006GL025766.

Enfield, D. B., A. M. Mestas-Nunez, and P. J. Trimble, 2001: The Atlantic multidecadal oscillation and its relation to rainfall and river flows in the continental US. *Geophys. Res. Lett.,* **28,** 2077–2080.

Feng, S., R. J. Oglesby, C. M. Rowe, D. B. Loope, and Q. Hu, 2008: Pacific and Atlantic SST influences on medieval drought in North America simulated by Community Atmospheric Model. *J. Geophys. Res.,* **113,** D11101, doi:10.1029/2007JD009347.

——, Q. Hu, and R. J. Oglesby, 2011: Influence of Atlantic sea surface temperature on persistent drought in North America. *Climate Dyn.,* **37,** 569–586, doi:10.1007/s00382-010-0835-x.

Frankignoul, C., 1985: Sea-surface temperature anomalies, planetary-waves, and air-sea feedback in the middle latitudes. *Rev. Geophys.,* **23,** 357–390.

Gray, S. T., L. J. Graumlich, J. L. Betancourt, and G. T. Peterson, 2004: A tree-ring based reconstruction of the Atlantic multidecadal oscillation since 1567 AD. *Geophys. Res. Lett.,* **31,** L12205, doi:10.1029/2004GL019932.

Higgins, R. W., Y. Yao, E. S. Yarosh, J. E. Janowiak, and K. C. Mo, 1997: Influence of the Great Plains low-level jet on summertime precipitation and moisture transport over the central United States. *J. Climate,* **10,** 481–507.

Hoerling, M., and A. Kumar, 2003: The perfect ocean for drought. *Science,* **299,** 691–694.

Holton, J. R., 2004: *An Introduction to Dynamic Meteorology.* 4th ed. International Geophysics Series, Vol. 88, Elsevier Academic Press, 535 pp.

Hu, Q., and S. Feng, 2001: Climatic role of the southerly flow from the Gulf of Mexico in interannual variations in summer rainfall in the central United States. *J. Climate,* **14,** 3156–3170.

——, and ——, 2007: Decadal variation of the southwest U.S. summer monsoon circulation and rainfall in a regional model. *J. Climate,* **20,** 4702–4716.

——, and ——, 2008: Variation of North American summer monsoon regimes and the Atlantic multidecadal oscillation. *J. Climate,* **21,** 2373–2383.

——, and ——, 2012: AMO- and ENSO-driven summertime circulation and precipitation variations in North America. *J. Climate,* **25,** 6477–6495.

——, ——, and R. J. Oglesby, 2011: Variations in North American summer precipitation driven by the Atlantic multidecadal oscillation. *J. Climate,* **24,** 5555–5570.

Kalnay, E., and Coauthors, 1996: The NCEP/NCAR 40-Year Reanalysis Project. *Bull. Amer. Meteor. Soc.,* **77,** 437–471.

Kerr, R. A., 2000: A North Atlantic climate pacemaker for the centuries. *Science,* **288,** 1984–1986.

Kistler, R., and Coauthors, 2001: The NCEP–NCAR 50-Year Reanalysis: Monthly means CD-ROM and documentation. *Bull. Amer. Meteor. Soc.,* **82,** 247–267.

Knight, J. R., R. J. Allan, C. K. Folland, M. Vellinga, and M. E. Mann, 2005: A signature of persistent natural thermohaline circulation cycles in observed climate. *Geophys. Res. Lett.,* **32,** L20708, doi:10.1029/2005GL024233.

Kushnir, Y., W. A. Robinson, I. Blade, N. M. J. Hall, S. Peng, and R. Sutton, 2002: Atmospheric GCM responses to extratropical SST anomalies: Synthesis and evaluation. *J. Climate,* **15,** 2233–2256.

Latif, M., and T. P. Barnett, 1994: Causes of decadal climate variability over the North Pacific and North America. *Science,* **266,** 634–637.

Lau, N. C., and M. J. Nath, 1994: A modeling study of the relative roles of tropical and extratropical SST anomalies in the variability of the global atmosphere ocean system. *J. Climate,* **7,** 1184–1207.

——, and ——, 1996: The role of the ''atmospheric bridge'' in linking tropical Pacific ENSO events to extratropical SST anomalies. *J. Climate,* **9,** 2036–2057.

Liang, X.-Z., L. Li, A. Dai, and K. E. Kunkel, 2004: Regional climate model simulation of summer precipitation diurnal cycle over the United States. *Geophys. Res. Lett.,* **31,** L24208, doi:10.1029/2004GL021054.

McCabe, G. J., M. A. Palecki, and J. L. Betancourt, 2004: Pacific and Atlantic Ocean influences on multidecadal drought frequency in the United States. *Proc. Natl. Acad. Sci. USA,* **101,** 4136–4141, doi:10.1073/pnas.0306738101.

Mestas-Nunez, A., and D. B. Enfield, 1999: Rotated global modes of non-ENSO sea surface temperature variability. *J. Climate,* **12,** 2734–2746.

Mo, K. C., J. N. Paegle, and R. W. Higgins, 1997: Atmospheric processes associated with summer floods and droughts in the central United States. *J. Climate,* **10,** 3028–3046.

——, J. E. Schemm, and S. Yoo, 2009: Influence of ENSO and the Atlantic multidecadal oscillation on drought over the United States. *J. Climate,* **22,** 5962–5982.

Namias, J., 1959: Recent seasonal interactions between North Pacific waters and the overlying atmospheric circulation. *J. Geophys. Res.,* **64,** 631–646.

——, 1965: Macroscopic association between monthly mean sea surface temperature and overlying winds. *J. Geophys. Res.,* **70,** 2307–2318.

——, 1969: Seasonal interactions between the North Pacific Ocean and the atmosphere during the 1960s. *Mon. Wea. Rev.,* **97,** 173–192.

——, X. Yuan, and D. R. Cayan, 1988: Persistence of North Pacific sea surface temperature and atmospheric flow patterns. *J. Climate,* **1,** 682–703.

Rasmusson, E. M., 1967: Atmospheric water vapor transport and water balance of North America. I. Characteristics of water vapor flux field. *Mon. Wea. Rev.,* **95,** 403–426.

Rudolf, B., and U. Schneider, 2005: Calculation of gridded precipitation data for the global land-surface using in-situ gauge observations. *Proc. Second Workshop of the International Precipitation Working Group,* Monterey, France, EUMETSAT, 231–247.

——, T. Fuchs, U. Schneider, and A. Meyer-Christoffer, 2003: Introduction of the Global Precipitation Climatology Centre (GPCC). Deutscher Wetterdienst Rep., 16 pp.

——, C. Beck, J. Grieser, and U. Schneider, 2005: Global precipitation analysis products. DWD Global Precipitation Climatology Centre (GPCC) DWD Internet Publication, 8 pp.

Ruiz-Barradas, A., and S. Nigam, 2005: Warm season rainfall variability over the U.S. Great Plains in observations, NCEP and ERA-40 reanalyses, and NCAR and NASA atmospheric model simulations. *J. Climate,* **18,** 1808–1830.

Schubert, S. D., M. J. Suarez, P. J. Pegion, R. D. Koster, and J. T. Bacmeister, 2004: On the cause of the 1930s Dust Bowl. *Science,* **303,** 1855–1859.

——, and Coauthors, 2009: A U.S. CLIVAR project to assess and compare the responses of global climate models to drought-related SST forcing patterns: Overview and results. *J. Climate,* **22,** 5251–5272.

Seager, R., Y. Kushnir, M. Visbeck, N. Naik, J. Miller, G. Krahmann, and H. Cullen, 2000: Causes of Atlantic Ocean climate variability between 1958 and 1998. *J. Climate,* **13,** 2845–2862.

Skamarock, W. C., J. B. Klemp, J. Dudhia, D. O. Gill, D. M. Barker, W. Wang, and J. G. Powers, 2007: A description of the advanced research WRF version 2. NCAR Tech. Note NCAR/TN-468+STR, 88 pp.

Sutton, R. T., and D. L. R. Hodson, 2005: Atlantic Ocean forcing of North American and European summer climate. *Science,* **309,** 115–118, doi:10.1126/science.1109496.

——, and ——, 2007: Climate response to basin-scale warming and cooling of the North Atlantic Ocean. *J. Climate,* **20,** 891–907.

Ting, M. F., and H. Wang, 1997: Summertime U.S. precipitation variability and its relation to Pacific sea surface temperature. *J. Climate,* **10,** 1853–1873.

Trenberth, K. E., and C. J. Guillemot, 1996: Physical processes involved in the 1988 drought and 1993 floods in North America. *J. Climate,* **9,** 1288–1298.

Tuttle, J. D., and C. A. Davis, 2006: Corridors of warm season precipitation in the central United States. *Mon. Wea. Rev.,* **134,** 2297–2317.

Veres, M. C., 2011: Atlantic multidecadal oscillation-forced regional summertime precipitation variations in the central United States. M.S. thesis, University of Nebraska Department of Earth and Atmospheric Sciences, 101 pp.

Wallace, J. M., 1975: Diurnal variations in precipitation and thunderstorm frequency over the conterminous United States. *Mon. Wea. Rev.,* **103,** 406–419.

Wang, C., S. Lee, and D. B. Enfield, 2008: Climate response to anomalously large and small Atlantic warm pools during the summer. *J. Climate,* **21,** 2437–2450.

Wang, H., S. Schubert, M. Suarez, and R. Koster, 2010: The physical mechanisms by which the leading patterns of SST variability impact U.S. precipitation. *J. Climate,* **23,** 1815–1836.